The morphology of symmetric diblock copolymers as revealed by neutron reflectivity

Spiros H. Anastasiadis, Thomas P. Russell, Sushil K. Satija, and Charles F. Majkrzak

Citation: The Journal of Chemical Physics **92**, 5677 (1990); doi: 10.1063/1.458499
View online: http://dx.doi.org/10.1063/1.458499
View Table of Contents: http://scitation.aip.org/content/aip/journal/jcp/92/9?ver=pdfcov
Published by the AIP Publishing

The morphology of symmetric diblock copolymers as revealed by neutron reflectivity

Spiros H. Anastasiadis and Thomas P. Russell[a)]
IBM Research Division, Almaden Research Center, 650 Harry Road, San Jose, California 95120-6099

Sushil K. Satija and Charles F. Majkrzak
National Institute of Standards and Technology, Reactor Radiation Division, Gaithersburg, Maryland 20899

(Received 21 September 1989; accepted 23 January 1990)

The specular reflectivity of neutrons has been used to characterize quantitatively the microphase separated morphology of symmetric, diblock copolymers of polystyrene (PS), and polymethylmethacrylate (PMMA), as a function of the total molecular weight of the copolymer where either block is perdeuterated. It is shown that the hyperbolic tangent function, as opposed to a linear or cosine-squared function, most closely describes the concentration gradient at the interface between the lamellar copolymer microdomains. The effective width of the interface is found to be independent of the molecular weight of the copolymer blocks and has a value of 50 ± 3 Å. This interface is also found to be identical to that between PS and PMMA, homopolymers. However, using measured values of the Flory–Huggins interaction parameter for PS and PMMA, current theoretical treatments cannot describe the observed widths of the interface.

I. INTRODUCTION

In block copolymers comprised of incompatible block segments, the chemical connectivity at the junction point leads to highly organized periodic domain microstructures on a size scale commensurate with the dimensions of the constituent polymer molecules.[1,2] Previous morphological studies[3–13] have investigated the nature of this microdomain structure in bulk specimens. For simple diblock copolymer melts, lamellar structures,[3–10] bicontinuous double diamond domains,[13] hexagonal arrays of cylinders, and body-centered-cubic arrays of spheres[3,11] are observed by changing the ratio of the molecular weights of the two components and/or the temperature. It has been recognized that the interface, i.e., the region between the adjacent microphases, is a major factor in determining many bulk properties and, moreover, is solely responsible for a number of unique phenomena (e.g., the yield stress in melts[14]). Thus, studies[4–6,8,15–20] have been aimed at providing information on the width of the interface and the composition variation across the interface. These investigations relied on information obtained by small-angle x-ray[4–6,8,16] and neutron scattering,[17] differential scanning calorimetry,[18] dynamic mechanical testing,[15] and transmission electron microscopy.[15,20]

For many of the applications of block copolymers the interfacial properties of the block copolymers are exploited. Thus, a fundamental understanding of the behavior of copolymers at surfaces and/or interfaces is essential. Despite this, only a few studies have appeared in the literature on block copolymers near surfaces[21–34] or interfaces.[35] These studies focused primarily on symmetric diblock copolymers which exhibit one-dimensional lamellar morphology in the bulk. Electron microscopy[28–30] has been used to reveal the arrangement of the microdomains at or near the surface and to obtain information on the size and the shape of the domains near the surface. An ordering of the lamellar microdomains parallel to the film surface has been observed and the domain at the free surface was found to be thinner than that observed in the bulk. Staining procedures, however, precluded quantitative treatment of the concentration of components at the surface. Experiments employing contact angle measurements[21] or x-ray photoelectron spectroscopy[22,23] have indicated that the lowest surface energy component preferentially segregates to the free surface of the sample. The ratio of the two components at the surface at equilibrium is found to vary depending upon the molecular weights of the constituent blocks.

Recently, dynamic secondary ion mass spectroscopy[31,32] (SIMS), neutron reflectivity[33] (NR), and interference microscopy[34] have shown that thin films of symmetric diblock copolymers of polystyrene (PS) and polymethylmethacrylate (PMMA) exhibit a strong orientation of the lamellar microdomains parallel to the surface of the film after annealing above the glass transition temperature. It was found that films cast from toluene solutions, while microphase separated,[36] showed no preferential alignment of the microdomains. However, subsequent annealing of the specimens above the glass transition temperature produced near-perfect orientation of the domains parallel to the surface.

In this article, neutron reflectivity has been used to investigate the morphology of symmetric, diblock copolymers of PS and PMMA. The orientation of the lamellar microdomains in combination with the sensitivity of neutron reflectivity is shown to yield details on the morphology of the copolymers unattained by other techniques. Investigations have been performed as a function of the molecular weight of the constituent blocks with attention focusing on the size

a) To whom correspondence should be sent.

 0021-9606/90/095677-15$03.00

and shape of the interface and its dependence on molecular weight. In addition, the size and shape of the interface separating PS and PMMA homopolymers and its relation to the interface seen in the corresponding diblock copolymers are discussed.

II. NEUTRON REFLECTIVITY

The fundamental principles of reflectivity have been extensively discussed in the literature.[37–42] For the studies of interest here, neutrons impinge upon a surface at a glancing angle θ and the reflected neutrons are detected at the corresponding angle θ from the surface. Thus, as shown in Fig. 1, this places the scattering vector in a direction normal to the surface. Reflectivities are reported as a function of the neutron momentum in vacuum, $k_{0,z}$, normal to the surface, i.e., in the z direction. $k_{0,z}$ is defined in terms of the wavelength of the neutrons, λ, as

$$k_{0,z} = \frac{2\pi}{\lambda} \sin\theta. \tag{1}$$

Thus, by variation of θ with λ fixed[33,42] or by variation of λ with θ fixed,[43–46] $k_{0,z}$ is varied. In a medium j comprised of nuclei with a scattering length per unit volume $(b/V)_j$ the refractive index η_j for neutrons is given by

$$\eta_j = \left[1 - \frac{\lambda^2}{2\pi}\left(\frac{b}{V}\right)_j\right]^{1/2}. \tag{2}$$

Consequently, the neutron momentum in medium j is given by

$$k_{j,z} = \left[k_{0,z}^2 - 4\pi\left(\frac{b}{V}\right)_j\right]^{1/2}. \tag{3}$$

The number of neutrons reflected at any interface will depend upon the difference in the neutron momenta in medium j and $j+1$. From classical Fresnel optics,[38,47,48] the reflectance or the reflection amplitude $r'_{j,j+1}$ at the interface is given by

$$r'_{j,j+1} = \frac{k_{j,z} - k_{j+1,z}}{k_{j,z} + k_{j+1,z}}. \tag{4}$$

In the case where there is a film deposited on a substrate, where the scattering length density varies within the film, the situation is more complicated. In fact, in only a few cases can an analytic solution of the reflectivity be obtained. Following the method of Parratt,[39] if the substrate is designated as the $j+1$ layer, the film is divided into j layers, each with a thickness d_j (not necessarily equal) and a scattering length density $(b/V)_j$. Provided d_j is small enough, the histogram of $(b/V)_j$ will closely approximate the actual variation of b/V in the specimen. Thus, for the layer adjacent to the substrate, the reflection coefficient is given by

$$r_{j-1,j} = \frac{r'_{j-1,j} + r'_{j,j+1}\exp(2id_jk_j)}{1 + r'_{j-1,j}r'_{j,j+1}\exp(2id_jk_j)}. \tag{5}$$

This reflection coefficient is then used to calculate the reflection coefficient of the $j-1$ layer by the recursion relation

$$r_{j-2,j-1} = \frac{r'_{j-2,j-1} + r_{j-1,j}\exp(2id_{j-1}k_{j-1})}{1 + r'_{j-2,j-1}r_{j-1,j}\exp(2id_{j-1}k_{j-1})}. \tag{6}$$

This recursion is then continued through the j layers in the specimen until the vacuum (air) reflection coefficient $r_{0,1}$ is obtained. The reflectivity R is then obtained from

$$R(k_0) = r_{0,1}r^*_{0,1}, \tag{7}$$

where $r^*_{0,1}$ is the complex conjugate of $r_{0,1}$.

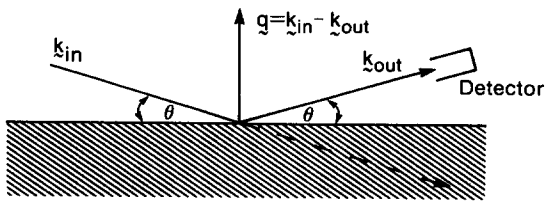

FIG. 1. Schematic diagram of a reflectivity experiment showing the direction of the incident and reflected beams and the direction of the neutron momentum transfer with respect to the surface of the specimen.

Alternatively, when the reflectivity is small ($< 10^{-3}$) the Born approximation can be used to show[41,42,49] that deviations from the Fresnel law of reflection at a sharp interface can be expressed as the square of the magnitude of the Fourier transform of the derivative of the scattering length density normal to the surface. Both approaches require modeling to evaluate the density profile normal to the surface with the exception of a few cases where analytical solutions are available. Equation (7) represents the Fresnel reflectivity, i.e., the reflectivity arising from a specimen and substrate with infinitely sharp boundaries. In general, surfaces possess a finite roughness which gives rise to a reduction in the measured reflectivity. This roughness can be directly incorporated into the recursion formulation so that different roughnesses at the air/sample and sample/substrate interfaces can be explicitly taken into account.

III. EXPERIMENT

Poly(styrene-*b*-methymethacrylate) symmetric, diblock copolymers where either the styrene or methylmethacrylate block was perdeuterated were used in this study. The copolymers purchased from Polymer Laboratories, Inc., were prepared anionically and were cleaned by successive washings in cyclohexane. This treatment removed the unreacted polystyrene homopolymer as evidenced by size exclusion chromatography. The characteristics of the copolymers are given in Table I. The use of the letter *d* prior to the block denotes perdeuteration of that block. For example, P(*d*-*S*-*b*-MMA) represents a diblock copolymer where the styrene block is perdeuterated. The molecular weights and polydispersities of the copolymers were determined from size exclusion chromatography measurements in reference to polystyrene standards. The characteristics of the polystyrene blocks were determined by extraction of a specimen after the first stage of the synthesis. The characteristics of the PMMA blocks were determined essentially from the difference between those of the copolymer (taking into account the differences in elution volumes between polystyrene and polymethylmethacrylate) and those of the polystyrene block.

TABLE I. Characterization of materials.

Copolymer	$M_{w,PS}$	$M_{w,PMMA}$	N_{PS}	N_{PMMA}	f_{PS}	M_w/M_n
P(*S-b-d*-MMA) 30 K	14 670	15 107	141	140	0.50	1.10
P(*d-S-b*-MMA) 100 K	52 900	48 000	472	480	0.50	1.07
P(*S-b-d*-MMA) 120 K	56 300	65 000	541	602	0.47	1.12
P(*d-S-b*-MMA) 300 K	169 500	131 900	1513	1319	0.53	1.08
d-PS	110 000	···	982	···	···	1.07
PMMA	···	107 000	···	1070	···	1.10

Specimens for the neutron reflectivity studies were prepared by dissolving the copolymer in toluene, a good solvent for both blocks, fully coating the substrate with the copolymer solution, and spinning the substrate at 2×10^3 rpm until a dry film was left on the surface. The specimens were then placed at 60 °C under vacuum to remove the solvent. After the investigation of the dried film, the specimens were annealed at 170 °C for 72–96 h to allow the specimens to equilibrate. They were subsequently cooled and investigated at room temperature. The total thickness of the specimens, typically $(1–2)\times10^3$ Å, depends upon the initial solution concentration, the molecular weight of the polymer, and the spinning speed.

Two different substrates were used in these studies. Experiments were initially performed using fused silica substrates ($76\times25\times13$ mm) polished to $\lambda/4$, where $\lambda\cong4300$ Å. Subsequent measurements were performed on silicon disks polished to $\lambda/4$ having the (100) crystal face on the surface with overall dimensions of 100 mm diameter and 5 mm thickness. In terms of the neutron reflectivity results discussed herein, either substrate yielded identical results. However, in terms of the sample preparation, the high optical reflectivity of silicon provided a rapid and direct means of evaluating the optical quality of the specimen.

Perdeuterated polystyrene (*d*-PS, $M_n = 100\,000$, $M_w/M_n = 1.07$) and polymethylmethacrylate (PMMA, $M_n = 107\,000$, $M_w/M_n = 1.10$) were purchased from Polymer Laboratories, Inc., and were used as received. The specimen used for the neutron reflectivity studies on the interfacial thickness between homopolymers was prepared as follows. The PMMA homopolymer was coated from toluene solution onto a polished Si (100) disk (50 mm diam, 5 mm thick). The film ($\sim$2000 Å) was annealed at 170 °C for 24 h to remove the solvent and to allow the PMMA molecules to relax. A *d*-PS ($\sim$1000 Å in thickness) film was prepared from toluene solution on a 50 mm $\times$ 75 mm glass microscope slide. After evaporation of the solvent, the sides of the microscope slide were scored with a razor blade and the film was floated off onto a pool of deionized water. The substrate with the PMMA was then used to pick up the *d*-PS film, thus making a bilayered specimen. The specimen was subsequently annealed under vacuum for 48 h at 170 °C to allow suitable time for the polymers to equilibrate within the bulk of the film and at the interface between the two layers.

Neutron reflectivity measurements were performed on the BT-4 triple-axis diffractometer at the reactor experimental hall of the National Institute of Standards and Technology. The experimental arrangement is shown in Fig. 2. The collimated neutron beam from the reactor is monochromated using pyrolytic graphite to obtain neutrons with a wavelength $\lambda = 2.35$ Å. The mosaic spread of the graphite monochromator is 0.667° yielding $\Delta\lambda/\lambda = 0.02$. Two cadmium slits (0.254 mm and 0.075 mm separated by 483 mm) located before the specimen reduced the angular divergence of the incident beam to $\sim$0.02°. A 2 mm slit (330 mm after the specimen) restricts the acceptance angular of the detector to $\sim$0.35°. A ^{3}He gas-filled detector is used to measure both the incident and reflected beams.

The importance of a perfect sample alignment with respect to the incident beam should be emphasized since the entire angular range covered during the experiments is from 0° to 1.7°. The sample rotation should be at the center of the neutron beam and at $\theta = 0°$ the neutron beam should be parallel to the surface of the specimen. The zero angle for the detector is first specified by measuring the angular spread of the incident radiation and positioning the detector such that the detected beam is symmetric around $2\theta = 0°$. Under these conditions the count rate of the incident beam is $\sim6\times10^3$ counts/s. A nearly nonreflecting flat lucite slab was then placed into the sample position. The slab is rotated in θ space to maximize the detected intensity. It is then translated into the incident beam until the detected intensity is one-half that of the direct beam. This procedure is repeated until one-half of the beam is blocked and any rotation of the slab in θ decreases the intensity. A well-characterized Ni mirror is then placed in the sample stage and its reflectivity profile is measured to verify the alignment and to measure the instrumen-

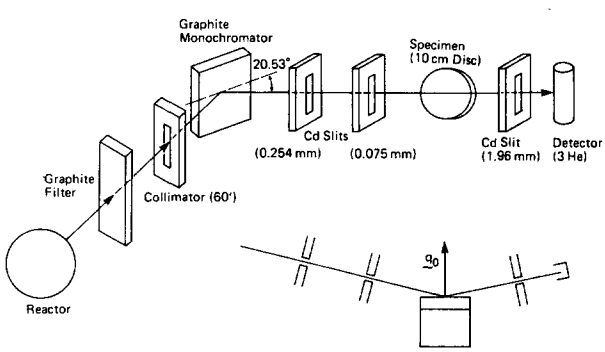

FIG. 2. Schematic diagram of the experimental geometry for the reflectivity experiment. Details are discussed in the text.

tal resolution. It should be noted that finite instrumental resolution causes a smearing of the reflectivity profile. The size of the neutron beam as well as the sample size were such that the specimen fully intercepted the beam at angles just below the critical angle (typically 0.10°). For each specimen investigated, fine adjustments are made in this angular range. With most specimens more than 92% (sometimes as much as 96%) of the incident beam was reflected at these angles.

Reflectivity profiles are obtained by rotating the sample to an angle θ and the detector to an angle 2θ maintaining the scattering vector normal to the surface. The background is measured with the detector offset from the specular position by $+0.6°$. The background is then subtracted from the raw data to obtain the specular reflectivity. This is of importance mainly at high angles where the specular reflectivity is low, on the order of 10^{-5} or less.

As mentioned above, instrumental resolution causes smearing of the reflectivity profile. Rather than desmearing the measured reflectivity profile the resolution function is convoluted with the theoretically calculated reflectivity profiles. The resolution function is assumed to be Gaussian with a full width at half-maximum of δk_0. In terms of measurable quantities, for small θ,

$$\frac{\delta k_0}{k_0} = \frac{\delta\theta}{\theta} + \frac{\delta\lambda}{\lambda}. \tag{8}$$

Therefore,

$$\delta k_0 = \frac{2\pi}{\lambda}\delta\theta + \frac{k_0}{\lambda}\delta\lambda. \tag{9}$$

Thus, for each value of k_0, δk_0 is given in terms of $\delta\theta$, $\delta\lambda$, and k_0. It should be noted that δk_0 increases with increasing k_0.

IV. RESULTS AND DISCUSSION

The reflectivity profile for the P(*S*-*b*-*d*-MMA) 30 K copolymer on fused silica prior to annealing is shown in Fig. 3 as a function of k_0, the projection of the incident neutron momentum onto the surface normal. As can be seen, the reflectivity profile at small values of k_0 exhibits total external reflection below the critical value of k_0 and then decreases as k_0 increases. The most pronounced feature of the profile is the high-frequency oscillation resulting from interference of the neutrons reflected at the air/polymer and polymer/substrate interfaces. From Eq. (5), for a single-layered specimen the frequency of the oscillation is directly related to the total film thickness. The solid line is the calculated reflectivity curve for a 1140 Å film with a uniform scattering length density of 4.2×10^{-6} Å^{-2} (the average scattering length density of the film weighted according to the number of PS and *d*-PMMA segments) over an infinitely thick fused silica substrate with $b/V = 3.4\times10^{-6}$ A^{-2}. The roughness at the copolymer/silica and copolymer/air interfaces could be represented by an error function. The root-mean-square values of the roughnesses used in the calculations are given in Table III as σ_{s_i} and σ_{A_i}, respectively. These roughnesses were incorporated into the density profile directly.

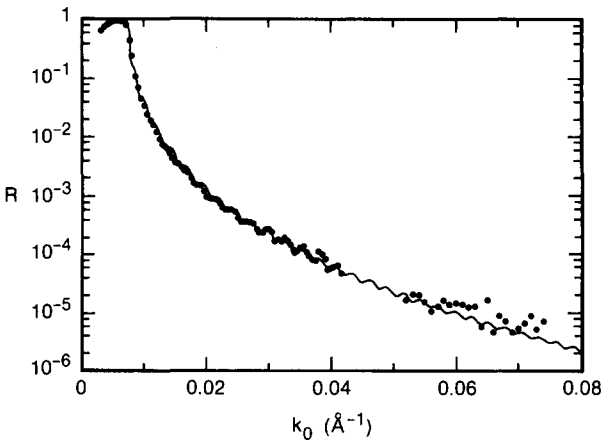

FIG. 3. Neutron reflectivity as a function of the neutron momentum normal to the surface, $k_{z,0}$, for a thin film of P(*S*-*b*-*d*-MMA) 30 K diblock copolymer on fused silica prior to annealing. The solid line is the calculated reflectivity profile.

Annealing the specimen at 170° for ~22 h followed by quenching to room temperature produced the reflectivity profile shown in Fig. 4. As discussed previously,[33] the three orders of Bragg reflections observed arise from the orientation of the PS and *d*-PMMA lamellar microdomains parallel to the substrate surface effectively producing a multilayered morphology within the film.[31,32] The solid line in Fig. 4 is the calculated reflectivity profile using the scattering length density profile shown in the inset. In this inset, as with all others, the air/polymer interface occurs at $z = 0$. The scattering length density of air or vacuum is essentially zero. The period of the multilayered structure is 175 Å in good agreement with small-angle scattering data from bulk specimens.[36] Within the precision of the data and assuming a cosine-squared gradient between the PS and *d*-PMMA mi-

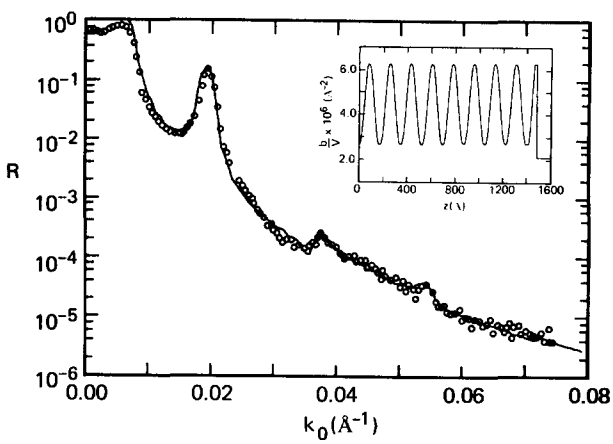

FIG. 4. Neutron reflectivity as a function of $k_{z,0}$ for a thin film of P(*S*-*b*-*d*-MMA) 30 K diblock copolymer on a Si substrate after annealing at 170 °C for 22 h. The inset shows the scattering length density profile normal to the film surface that was used to calculate the reflectivity profile shown as the solid line.

crodomains, the interfacial thickness is found to be 50 ± 2 Å. It should be noted that variation of the width of the interface outside of these limits produced severe deviations from the observed reflectivity. Such precision on the interfacial width has been, heretofore, unattainable by other techniques. For example, analysis of the deviations of small-angle x-ray scattering data from Porod's law at high scattering vectors,[50] while in agreement with the finding here, could only estimate that the interfacial width for this particular copolymer is ~ 50 Å. It should also be noted that for this specimen, due to the size of the interface relative to the domain size, the exact functional form of the composition variation at the interface could not be assessed. This refinement, as will be shown, is possible with the higher molecular weight block copolymers.

In agreement with previous studies[23,31,32] PS is shown to be preferentially located at the air/copolymer interface, due to the lower surface energy of PS, and *d*-PMMA is preferentially located at the Si surface due, most likely, to interactions between the more polar PMMA and the thin native oxide layer at the Si surface. Electron microscopy studies on poly(styrene-*b*-isoprene) copolymers[28] have shown that the layer nearest the air interface is thinner than the respective layers in the bulk. Examination of the density profile in the inset shows that the thickness of the layers adjacent to the air/polymer and polymer/substrate interfaces are precisely one-half that of the respective inner layers. Finally, the individual lamellar microdomains are not pure PS or *d*-PMMA but rather are comprised of mixture of both components. Volume fraction ratios of 0.76/0.24 and 0.10/0.90 for PS/*d*-PMMA, respectively, were found. This is consistent with the copolymer being in the weak segregation limit. Note, also, that the interface between PS and *d*-PMMA microdomains occupies nearly 62% of the entire specimen volume.

Independent confirmation of the model derived from the neutron reflectivity can be obtained from angle-resolved x-ray photoelectron spectroscopy (XPS). Over the first 70 Å from the air/polymer interface the PS/*d*-PMMA ratio can be assessed from the relative intensities of the C_{1s} and O_{1s} electron peaks. The sampling depth of XPS, z, is given by $z = 3\lambda' \cos\theta'$, where λ' is the electron mean free path which is 23 ± 3 Å for polymers[51,52] and θ' is the takeoff angle of the electron with respect to the surface normal. Thus, variation of θ' allows different depths to be probed. From the neutron reflectivity studies a model of the composition $\phi(z)$ with respect to the depth into specimen z is obtained. Consequently, for a known $\phi(z)$ the expected XPS signal at an angle θ' can be calculated by

$$\omega(\theta') = \frac{\int_0^\infty \phi(z)\exp[-z/(\lambda' \cos\theta')]dz}{\int_0^\infty \exp[-z/(\lambda' \cos\theta')]dz}. \quad (10)$$

A comparison between the measured XPS signal and that calculated from the model derived from the neutron reflectivity data using Eq. (10) are shown in Table II. As can be seen, the agreement between the two is very good.

An important aspect of the oriented lamellar microdomain morphology is their flatness. If the lamellar microdomains are not parallel to the surface or if there is a conformal or other waviness of the lamellae, the interfacial width will appear broader than it actually is. In performing so-called longitudinal scans, where the direction of the scattering vector remains normal to the substrate while its magnitude $|\mathbf{q}| = |\mathbf{k}_f - \mathbf{k}_i| = (4\pi \sin\theta)/\lambda = 2k_{0,z}$ is changed incrementally, neutron plane waves in effect average over slabs of thickness dz which may be inhomogeneous. The lateral extent (parallel to the substrate surface) over which this averaging occurs is determined by the overall thickness of the film, the angle of incidence θ, and the longitudinal instrumental resolution δq determined by the spectrometer configuration. In our arrangement with an effectively open detector following the sample, δq is given by Eq. (9) which can be rewritten in terms of q as

$$\delta q = \frac{\delta\lambda}{\lambda} q + \frac{4\pi}{\lambda}\left[1 - \left(\frac{q\lambda}{4\pi}\right)^2\right]^{1/2} \delta\theta, \quad (11)$$

where $\delta\lambda/\lambda$ is a measure of the monochromaticity of the incident radiation and $\delta\theta$ is the angular divergence of the incident beam [full width at half-maximum (FWHM)]. However, if the sample is made up of blocks of parallel lamellae where each block is of sufficient lateral extent to coherently reflect incident neutrons independently of other blocks, then an angular distribution of individual block orientations relative to the substrate normal will produce an additional broadening in $\delta\theta$. If the scattering angle 2θ were sufficiently well defined by a pair of apertures following the sample, then a rocking curve or scan of θ at a fixed 2θ or q corresponding to the multilayer Bragg peak would give, upon deconvolution of the instrumental component, the contribution of such an angular distribution of blocks of lamellae. However, in the geometry used here with the detector open, such a scan cannot be performed since q is determined soley by the θ, assuming the scattered radiation is predominantly specular in nature. (A θ:2θ motion of sample and detector is still performed in practice, since the detector window is not wide enough to simultaneously cover the entire angular range scanned.) Nonetheless, an upper limit on the width of any angular distribution intrinsic to the sample can be obtained from the peak width Γ_m measured in the longitudinal scan provided the instrumental resolution δq is known. To compute the angular component attributable to the sample, we first write

$$\Gamma_I = (\Gamma_m^2 - \Gamma_s^2)^{1/2}, \quad (12)$$

where Γ_I is an *effective* instrumental width containing contributions from both beam divergence and a possible lateral nonuniformity of the sample, and where Γ_s is the minimum width to be expected for an ideal (i.e., perfectly flat and regular) sample. In the present case with a specimen thick-

TABLE II. Surface concentration of P(*S-b-d*-MMA) 30 K.

Takeoff angle (deg)	Penetration depth (Å)	ω_{XPS}	$\omega_{reflectivity}$
30	60	0.66	0.70
55	40	0.76	0.74
80	12	0.77	0.76

ness of 1400 Å, $\Gamma_s \simeq 2\pi/1400$ Å $= 0.0045$ Å^{-1}. For the observed multilayer Bragg peak at $q = 0.042$ Å^{-1} with $\Gamma_m = 0.0056$ Å^{-1}, we obtain $\Gamma_I \simeq 0.0033$ Å^{-1}. We can therefore write

$$\Gamma_I = \delta q + \frac{4\pi}{\lambda}\left[1 - \left(\frac{q\lambda}{4\pi}\right)^2\right]^{1/2} \delta\theta_s, \tag{13}$$

where δq is given by Eq. (11) in which $\delta\theta$ pertains only to the angular divergence of the beam, whereas $\delta\theta_s$ in Eq. (13) represents the angular distribution of lamellar blocks in the sample. For $\Gamma_I = 0.0033$ Å^{-1} and $\delta q = 0.002\,74$ Å^{-1}, $\delta\theta_s \simeq 0.006°$. This upper limit estimate is consistent with optical interference microscopy results on these same specimens.[32]

Now for $\Gamma_I = 0.0033$ Å, the spatial extent along $\mathbf{q} \| z$ for which coherent scattering from a structure can be measured is of the order $2\pi/\Gamma_I \simeq 1900$ Å, which is greater than the overall sample thickness in the present case. What length scale does this imply laterally? For $q = 0.042$ Å^{-1} and $\lambda = 2.35$ Å, $\theta \simeq 0.45°$, so that the lateral distance between an atomic scattering center at the top of the film and one at the bottom, which are excited by the same incident neutron plane wave, is approximately 24.2 μm as depicted schematically in Fig. 5. This means that if blocks of lamellae are present, they must be at least 24 μm wide to reflect coherently the neutrons independently of one another.

To determine whether the lamellae are wavy or the interfaces are discontinuous within a coherently reflecting region or block, a longitudinal scan with $\mathbf{q}$ parallel to the plane of the substrate at $q_z = 0$ can, in principle, be performed. It should be noted that with well-defined collimation preceding the detector, a rocking curve or transverse q scan through the multilayer Bragg peaks also gives some information about interfacial roughness. However, the *transverse* width of the Bragg reflection profile at $q_z = 2\pi/D$, where D is the bilayer period, is practically the same whether each layer is perfectly homogeneous or composed of a distribution of blocks of varying scattering density. The scattering due to any interfacial roughness appears superimposed as a significantly broader and weaker profile. Although we have not yet performed measurements with $\mathbf{q}$ parallel to the plane of the multilayer because of the experimental degree of difficulty, the importance of such measurements is realized. Such measurements will be performed if samples adequate for this purpose can be prepared.

The reflectivity profile obtained for the P(*d*-*S*-*b*-MMA) 100 K copolymer annealed at 170 °C for 37 h under vacuum is shown in Fig. 6. Due to the increase in the molecular weight, which results in a larger period, and the orientation of the lamellar microdomains with respect to the surface, seven orders of Bragg reflections are clearly evident. As in the previous data, the relative heights of the different reflections will be associated with the volume fractions of the *d*-PS and PMMA microdomains, the lateral coherence of the multilayers, the purity of the phases, and, particularly at higher scattering vectors, the width of the interface between the microdomains. The solid line in Fig. 6 is the calculated reflectivity curve using the scattering length density profile shown in the inset. As can be seen the calculated profile

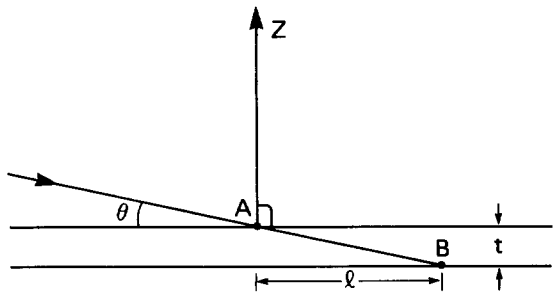

FIG. 5. A neutron plane wave incident upon a specimen at an angle θ excites spherical waves for atoms A and B on the top and bottom of the film, respectively, which are separated by a distance $l = t/\tan\theta$ (in the kinematic diffraction limit). The spherical wavelets emanating from these and other atoms of the film excited by the same neutron plane wave can coherently interfere to create an outgoing reflected neutron plane wave for a properly ordered multilayer structure.

reproduces the experimental reflectivity curve remarkably well over nearly 6 orders of magnitude in the reflected intensity. The multilayered structure is composed of 3.5 periods each with 210 Å *d*-PS and 188 Å PMMA microdomains, which is consistent with the relative volume fraction of the two blocks. The interfacial profile between the microdomains is well represented by a hyperbolic tangent function with an effective width of 50 Å. Thus, the volume fraction of the total specimen that is occupied by the interface is ~ 0.25. As before, *d*-PS is preferentially located at the air/copolymer interface and PMMA is preferentially located at the copolymer/Si interface. Once more, the thickness of the layers adjacent to the air/polymer and polymer/substrate interfaces are exactly one-half that of the respective layers of the underlying multilayer structure. The scattering length densities of the two phases correspond to those of pure *d*-PS and PMMA using bulk densities, which is in keeping with the observation that this copolymer, due to the increase in molecular weight, is in the strong segregation limit.

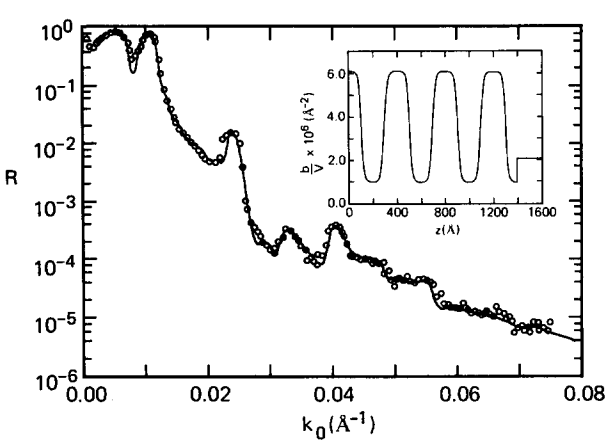

FIG. 6. Neutron reflectivity as a function of $k_{z,0}$ for a thin film of P(*d*-*S*-*b*-MMA) 100 K copolymer annealed at 170 °C for 37 h. The points are the measured data, whereas the solid line is that calculated using the scattering length density profile shown in the inset. The substrate in this case is Si.

For the low molecular weight block copolymer, it was not possible to specify the exact functional form of the interfacial gradient due to the small number of Bragg reflections in the experimentally accessible scattering vector range. For the P(*d*-*S*-*b*-MMA) 100 K specimen, however, the hyperbolic tangent function yielded a far better description of the observed reflectivity profile than either a linear or a cosine-squared function. Figure 7 shows a comparison between the best fit obtained with a linear interfacial profile and a hyperbolic tangent function. Clearly, the calculated profile using the linear profile overestimates the heights of the peaks and the minima of the measured reflectivity curve. Thus, to within the precision of the data, a hyperbolic tangent functional form of the interfacial profile with a width of 50 ± 3 Å mast accurately reproduces the observed data. This cannot be taken as unequivocal proof that the interfacial profile has a hyperbolic tangent functional form. Any profile that very closely approximates a hyperbolic tangent would reproduce the data equally well.

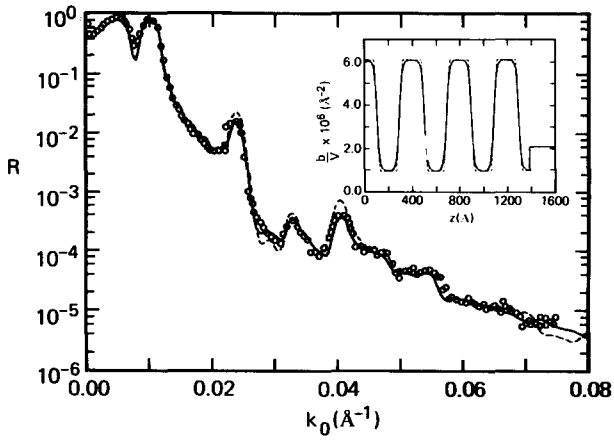

FIG. 7. Comparison of the experimentally measured neutron reflectivity profile and those calculated using a linear (---) and hyperbolic tangent (—) function to describe the segment density profile at the interface between the PS and PMMA microdomains for P(*d*-*S*-*b*-MMA) 100 K.

The data in Fig. 7 can also be used to assess the uniformity of the sizes of the individual lamellae comprising the multilayer. Direct calculations where the average size of the microdomains was varied about an average, e.g., the introduction of a microdomain size distribution, resulted in poor agreement between the calculated and measured profiles. An estimate of the size distribution can be obtained by assuming that there is a disorder in the multilayer that can be characterized using paracrystalline lattice statistics.[6,8,53] If $g = \Delta L / \overline{L}$, where ΔL is the standard deviation of L from the average value $\overline{L}$ assuming a Gaussian size distribution, then, according to paracrystalline lattice theory, the nth order reflection will be distinguishable from the background if $gn \lesssim 0.35$. Therefore, for $n = 7$, $g \lesssim 0.05$. In terms of the heterogeneity of the size distribution of L, $\overline{L}^2/\overline{L} = (\Delta L / \overline{L})^2 + 1 \leqslant 1.0025$. The model of paracrystalline disorder is applicable only in the case when one has a large number of bilayers with an average thickness $\overline{L}$. Nevertheless, these results do indicate that the thickness distribution is quite small and that the microdomains are very uniform in size.

Earlier, it was mentioned that the PMMA microdomains are preferentially located at the Si/polymer interface due to the presence of a very thin native oxide layer on the Si surface. To investigate this further, the same copolymer [P(*d*-*S*-*b*-MMA) 100 K] was prepared on a fused silica substrate and annealed for 37 h at 170 °C. The measured reflectivity profile is shown in Fig. 8. The solid line corresponds to a calculated reflectivity curve using a model identical to that used in Fig. 6. An added feature of the reflectivity data in this case is the presence of a high-frequency oscillation arising from the total thickness of the specimen. This corresponds to precisely 3.5 periods. The fact that a single profile describes the data on the fused silica (which is essentially SiO_2), as well as the data on the Si substrate, is an indication that it is the presence of a thin SiO_2 layer on the Si surface that causes the preferential adsorption of the PMMA domain to the copolymer/substrate interface. This is also consistent with previous SIMS observations where it was found that coating of the Si surfaces with a layer of gold caused the PS microdomains to locate preferentially at both the air/polymer and the polymer/substrate interfaces.[32]

Finally, experiments were performed on the P(*d*-*S*-*b*-MMA) 300 K copolymer. However, this specimen required a special preparation. It has been seen previously[32] that the rate at which the lamellar microdomains orient parallel to the film surface depends strongly on the molecular weight of the copolymer. In fact, specimens of the P(*d*-*S*-*b*-MMA) 300 K, where the total thickness of the film was $\sim 2 \times 10^3$ Å, were not found to yield a well-oriented multilayered structure even after 240 h annealing at 170 °C under vacuum. While there is evidence that the lamellar microdomains will orient parallel with respect to the surface with further annealing, extensive annealing of the copolymer at these high

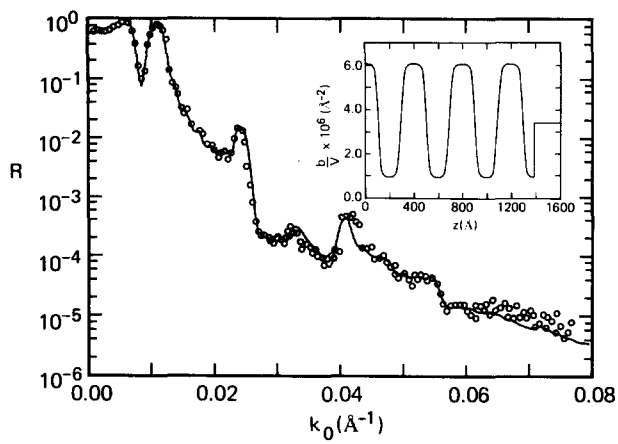

FIG. 8. Neutron reflectivity profile as a function of $k_{z,0}$ for a thin film of P(*d*-*S*-*b*-MMA) 100 K prepared on a fused silica substrate and annealed at 170 °C for 37 h. The points show the measured data, whereas the solid line is the calculated reflectivity profile using the scattering length density profile shown in the inset.

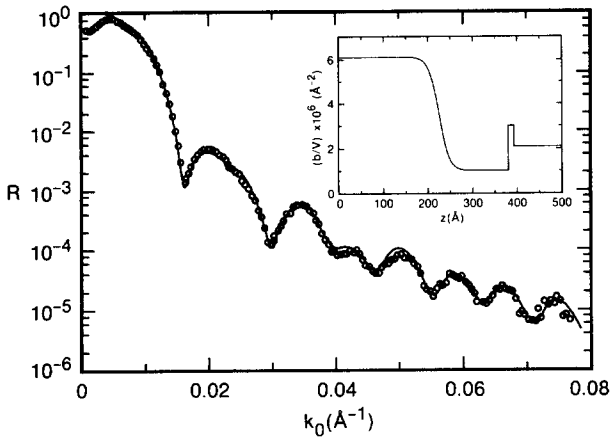

FIG. 9. Neutron reflectivity as a function of $k_{z,0}$ for a P(*d*-*S*-*b*-MMA) 300 K diblock copolymer annealed for 240 h at 170 °C. The film prepared on Si had a total thickness of 411 Å. The points are the measured data, whereas the solid line was calculated using the density profile shown in the inset.

temperatures could result in thermal degradation. Therefore, a film of the P(*d*-*S*-*b*-MMA) was prepared where the total thickness of the film was designed to correspond to one-half of the expected period. This specimen was then annealed at 170 °C for 240 h under vacuum. The neutron reflectivity profile of this specimen is shown in Fig. 9. As can be seen in the data there are at least two distinct oscillations evident in the reflectivity profile. One characterizes the total thickness of the film, whereas the other is associated with formation of a bilayer comprised of a layer of *d*-PS and PMMA. In fact, the scattering length density profile shown in the inset was used to calculate the reflectivity profile represented by the solid line in the figure. As can be seen, the data are well represented by the calculated profile.

Basically, the specimen can be described by a 255 Å layer of *d*-PS on top of a 156 Å layer of PMMA where the densities correspond to their respective bulk values. The gradient in the scattering length density between the *d*-PS and PMMA layers is well represented with the hyperbolic tangent function with an effective width of 50 ± 5 Å. As before, use of a linear gradient or a cosine-squared function to describe the interfacial region did not produce a satisfactory description of the observed reflectivity. While it is evident that a bilayer is formed, it is not clear, at this time, whether the results of this specimen represent precisely one-half of the true period for this copolymer. Currently, an investigation is underway to examine the effect of film thickness, where the thicknesses of the films are less than 1.5 periods of the copolymer morphology. It should be recalled that, due to the strong orientation of the lamellae and the preferential adsorption of PS to the air/copolymer interface and of PMMA to the copolymer/substrate interface, that the total film thickness is given by $(n + 1/2)L$, where L is the period and n is an integer.[31] If the film thickness deposited on the substrate is such that $n < 1$, as in the case here, there may be strong contributions from the surface energy that can perturb the morphology. However, the density profile derived from Fig. 9 is consistent with the multilayer data of the other, lower molecular weight specimens.

An additional feature in the scattering length density profile shown in Fig. 9 is the presence of an oxide layer. In fact, for the calculated profile a 20 Å oxide layer with a scattering length density of 3.0×10^{-6} Å^{-2} was necessary in order to describe the experimental results. This scattering length density is $\sim 10\%$ less than the typical value of the scattering length density of SiO_2 and may reflect a variation in structure of the oxide layer or a contamination of the oxide layer in this specimen. The introduction of an oxide layer was not necessary, however, to describe the data for the other copolymers. This is primarily due to the number of layers in the multilayer giving rise to the reflectivity. In the data for the lower molecular weight copolymers, numerous layers were evident and the contribution to the reflectivity from an oxide layer was minimal. However, in this case where there are only two layers and where PMMA has a scattering length density close to that of silicon, the contribution to the reflectivity from the oxide layer is significant.

The structural information obtained from the neutron reflectivity studies are summarized in Table III. Included in this tabulation are the period L, the width or thickness of the interface a_I, the volume fraction of the specimen occupied by the interface X_I ($= 2a_I/L$), and the average area occupied by a copolymer chain at the interface, S. This latter quantity

TABLE III. Characteristics of P(*S*-*b*-MMA) diblock copolymers measured by neutron reflectivity.

Copolymer	L_{PS}[a] (Å)	$(b/V)_{ps} \times 10^6$[b] (Å^{-2})	L_{PMMA}[c] (Å)	$(b/V)_{PMMA} \times 10^6$[b] (Å^{-2})	L (Å)	σ_{S_i}[d] (Å)	σ_{A_i}[e] (Å)	a_I (Å)	X_I	S (Å^2)
P(*S*-*b*-*d*-MMA) 30 K	91	2.7	84	6.25	175	6	4	50 ± 2	0.57	481
P(*d*-*S*-*b*-MMA) 100 K	210	6.1	188	1.0	398	6	4	50 ± 3	0.24	660
P(*S*-*b*-*d*-MMA) 120 K	268	1.43	244	6.8	512	4	4	48 ± 3	0.18	712
P(*d*-*S*-*b*-MMA) 300 K	450[f]	6.1	312[f]	1.0	762[f]	4	4	50 ± 5	0.12	1223

[a] Thickness of PS microdomain.
[b] $(b/V)_i$ is the scattering length density of microdomain i.
[c] Thickness of PMMA microdomain.
[d] Root-mean-squared roughness at the copolymer/substrate interface.
[e] Root-mean-squared roughness at the air/polymer interface.
[f] These values are twice that observed for the specimen studied assuming this was a half layer.

was calculated from $S = 2M_{PMMA}\nu_{PMMA}/(N_A L_{PMMA})$, where M_{PMMA} and ν_{PMMA} are the molecular weight and partial specific volume of the PMMA chains ($\nu_{PMMA} = 1/\rho_{PMMA}$), L_{PMMA} is the thickness of the PMMA layer, and N_A is the Avogadro's number. The PMMA chains were selected for this calculation in order to ensure that any traces of homopolymer PS that may remain in the samples, even after the cleaning, do not affect the calculation.

The copolymer periods obtained from the reflectivity studies are shown in Fig. 10 as a function of the total number of segments in the chain. It has been assumed that the period of the P(*d*-*S*-*b*-MMA) 300 K copolymer is twice that of the measured value. Plotted with these data are results from independent small-angle x-ray and neutron scattering studies. As can be seen, the period increases uniformly with the molecular weight. The best fit to these data, shown by the solid line in the figure, yields

$$L = 4.7N^{0.65} \tag{14}$$

where L is the period in angstroms and N is the total number of monomers in the copolymer. This result agrees with theoretical predictions, as will be discussed, where, for diblock copolymers in the strong segregation limit, L varies with $N^{0.66}$. The surprising feature of this result is that this relation accurately predicts the period of the P(*S*-*b*-*d*-MMA) 30 K copolymer which, according to our results, clearly shows that the copolymer is in the weak segregation limit. It should also be noted that Eq. (14) differs from our previous results where the data indicated that the period varied according to $N^{0.5}$, i.e., the copolymers are continually in the weak segregation limit.[36] The result of this previous study is shown as the dashed line in the figure. It is clear that the limited range of molecular weights available make absolute definition of the exponent rather difficult since minor scatter in the data can alter the value of the exponent. The results in Eq. (14) are, however, more reasonable for the higher molecular weight copolymers.

In Fig. 11 are shown the width of the interface and the volume fraction of the specimen occupied by the interface. The interfacial width a_I, to within experimental uncertainties, is independent of the copolymer molecular weight which is in agreement with the results of Hashimoto, Shibayama, and Kawai[6] on polystyrene/polyisoprene diblock copolymers although the interfacial widths for the copolymers studied here are much broader. As found previously, the volume fraction of the specimen occupied by the interface decreases strongly with the molecular weight. This is consistent with a diblock copolymer going from the weak to strong segregation limit with increasing molecular weight.

The interfacial area occupied by a block copolymer chain increases weakly with the molecular weight as

$$S = 48.6N^{0.39}, \tag{15}$$

where S is in units of Å^2. Both Eqs. (14) and (15) indicate that the copolymer chains adopt an extended configuration due to the constraints associated with the lamellar morphology. From Eq. (15) it is seen that the area per chain increases with increasing copolymer molecular weight. Conversely, the junction points, i.e., the point where the PS and

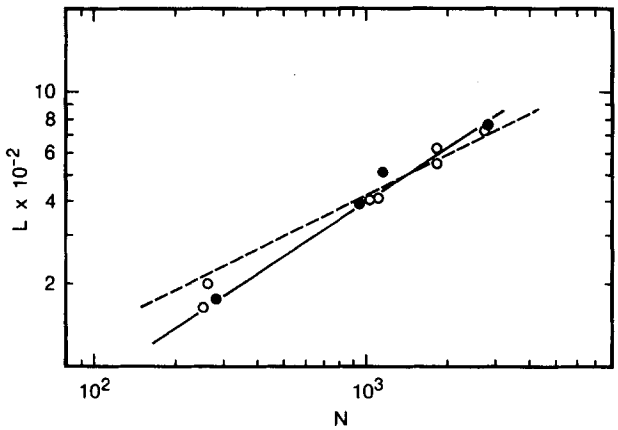

FIG. 10. The logarithm of the period of the lamellar microdomains as a function of the logarithm of the total number of segments in the copolymer. Both neutron reflectivity (●) and x-ray scattering (○) results (obtained from independent scattering studies) are shown in the figure. Best fit for an $N^{0.5}$ (---) behavior [obtained previously (Ref. 36)] and for an $N^{0.65}$ (—) behavior are shown.

PMMA blocks are chemically joined, occupy an increasingly minor portion of the interface so that for a copolymer with an infinite molecular weight the interface will be occupied almost strictly by nonbonded PS and PMMA segments which undergo segmental interactions at this interface. Consequently, in the infinite molecular weight limit, it is necessary that the interface of the copolymer be identical to the interface between layers of the corresponding homopolymers.

Neutron reflectivity was used to measure the interface between a layer of *d*-PS on top of a layer of PMMA. The reflectivity profile for this bilayer annealed for 48 h at 170 °C is shown in Fig. 12. The reflectivity profile exhibits a high-frequency oscillation corresponding to the thickness of the upper *d*-PS layer. The solid line in Fig. 12 corresponds to a calculated reflectivity profile where the thickness of the *d*-PS

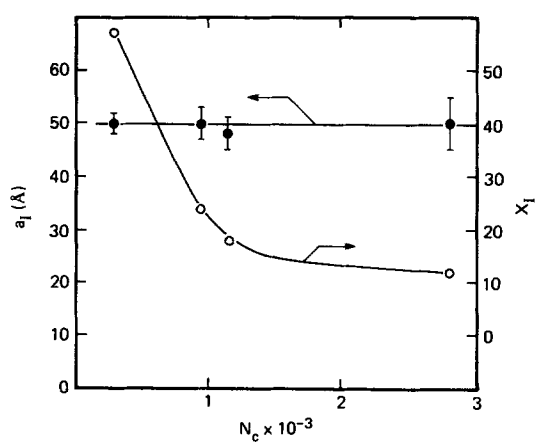

FIG. 11. The width of the interface between the PS and PMMA lamellar microdomains and the volume fraction of the specimen occupied by the interface as a function of the number of segments in the copolymer.

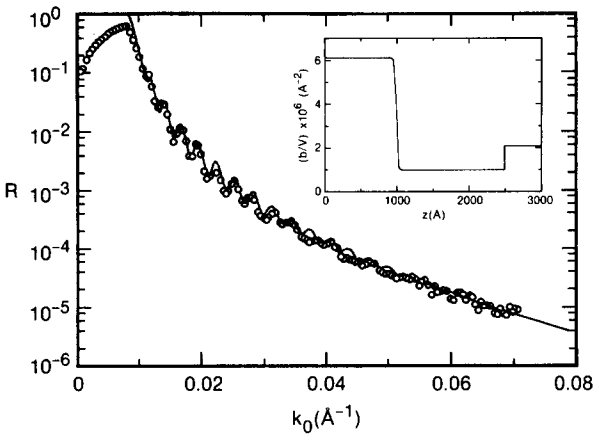

FIG. 12. Neutron reflectivity profile for a bilayer of deuterated polystyrene film on top of a normal polymethymethacrylate film. The bilayer, prepared on silicon, was annealed for 48 h at 170 °C. The solid line is the reflectivity profile calculated using the segment profile shown in the inset.

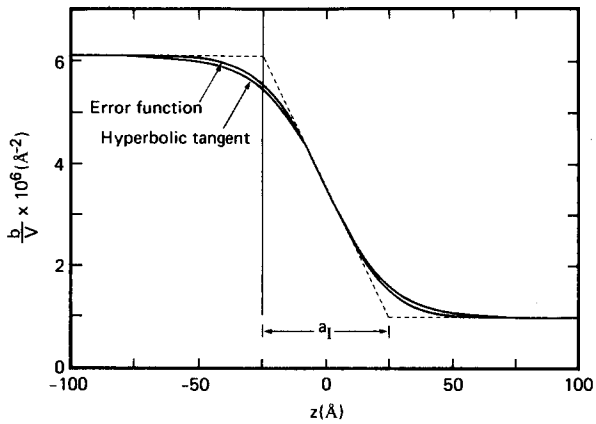

FIG. 13. A comparison of a hyperbolic tangent function where the effective width of the interface is 50 Å with the error function profile derived from a roughness parameter of 20 Å.

layer is 990 Å and that of the PMMA is ~2000 Å. Due to the thickness of the PMMA layer any oscillations associated with this thick layer occur at a frequency that is too high to be resolved. Effectively, the PMMA layer is infinitely thick. The interface between these two layers is well described by a hyperbolic tangent function with an effective width of 50 ± 5 Å. This value agrees with estimates based on an empirical relationship between the width of the interface and the interfacial tension given by Wu[54] using experimental values of the interfacial tension[55] for the PS/PMMA blend. Thus, for the molecular weights of the homopolymers studied, the interface between the homopolymer layer is identical to that seen in the case of the copolymer.

The results obtained in this work stand in apparent contrast to similar neutron reflectivity studies on bilayers of PS with *d*-PMMA by Fernandez *et al.*,[46] where a 200 Å layer of *d*-PMMA ($M_w = 220\,000$) was placed on a thick (~8000 Å) layer of PS ($M_w = 19\,200$). For both the "as-cast" specimen and a specimen annealed at 120 °C for 6 h an interface of 20 Å was found. It was found that $\Delta\theta$, the broadening associated with beam divergence and long-range waviness in the specimen, was found to increase from 0.08 to 0.14. This change must be associated with the long-range waviness in the specimen since the beam divergence should be invariant. This effect was not found in the studies here. It is necessary to examine the definitions of the interfacial width used to resolve the discrepancy between the two studies. In this work a tangent to the interface at the halfway point is drawn and extended to the concentrations corresponding to those of the microdomains. The projection of this distance onto a line running normal to the lamellae defines a_I. In the work by Fernandez *et al.*, a Debye–Waller factor was used to describe the roughness between the PS and PMMA layers, i.e., the reflectance of this interface was multiplied by $\exp(-2k_{PS}k_{PMMA}\langle\sigma^2\rangle)$ where k_i is the neutron momentum in layer i and $\langle\sigma^2\rangle^{1/2}$ is the root-mean-squared roughness at the PS and PMMA interfaces. In real space this corresponds to an error function with a shape very close to the hyperbolic tangent function used in our studies. A comparison between the two is shown in Fig. 13. Consequently, the roughness parameter σ must be multiplied by $\sqrt{2\pi}$ to yield a value for a_I that can be compared with theory. This factor brings their effective interface to 50 Å, which is in exact agreement with the results found here. This is noteworthy, given the different molecular weights used in the two studies and the differences in the sample preparation temperatures.

V. THEORETICAL TREATMENTS OF DIBLOCK COPOLYMERS

The theoretical models for the equilibrium properties of diblock copolymers can be divided into two major classes. The first class, the strong segregation limit theories,[56–70] are applicable to well-developed ordered microstructures. These theories are believed to be most accurate at low temperatures where the phases are purely one component and the widths of the interfaces between the microdomains are small relative to the size of the domains. The second class are the weak segregation limit theories[71–73] that are applicable to the disordered phase of copolymers and to the ordered microphases at temperatures very near the microphase separation temperature. The morphology of the diblock copolymers in the thin films is identical to that seen in the bulk with the exception of the strong orientation of the lamellar microdomains parallel to the surface of the substrate. Consequently, given the precision to which the period and interface width have been obtained in this study, quantitative comparisons can be made with the predictions of existing theories. Comparisons will be made with the "confined chain" model of Meier,[56–59] the "narrow interface approximation" theory of Helfand and Wasserman,[63–65] the theory of Ohta and Kawasaki,[67,68] and that of Semenov.[69]

Meier[56–59] modelled the domain structure by random-flight chains being constrained by barriers. The barriers represent the effect of incompatibility between the components and the restriction of the components to the microdomains.

Meier[56] identified the different contributions to the free-energy change related to the spatial constraints as (i) a change in the interfacial contact energy associated with the fact that, in the microphase separated state, contacts between the two components occur only at the interface; (ii) the placement entropy, i.e., an entropy loss associated with restricting the junction point to within a narrow region on the interface; and (iii) an entropy loss arising from the restriction of the block segments to their respective domain regions and with the perturbations of chain dimensions that occur when the block molecular weights are unequal. In the original formulation, Meier arbitrarily assumed that the interfacial profile had a cosine-squared functional form. In the latest version[59] the hyperbolic tangent functional form was used.

Using the notation in Fig. 14, Meier's theory can be summarized as follows. The interface parameter λ used by Meier is related to the interfacial thickness a_I as

$$a_I = \frac{1}{[d\phi_k(z)/dz]_{\phi_k=0.5}} = \frac{2}{\pi}\lambda. \tag{16}$$

The period of the microdomain morphology L is

$$L = T_A + T_B, \tag{17}$$

where T_i is the thickness of domain i. The requirement of maintaining uniform density in the domain space T_i' yields a relationship between T' and the unperturbed chain dimension

$$T_i' = 1.4\alpha_i \langle R_i^2 \rangle_0^{1/2}, \tag{18}$$

where α_i is the chain-expansion factor (along the lamellar normal) in the domain space caused by the constraint-volume and volume-filling effects and $\langle R_i^2 \rangle_0$ is the unperturbed mean-square end-to-end distance of chain i. T_i' is related to T_i by

$$T_i' = T_i + \zeta\lambda, \tag{19}$$

where ζ is an adjustable parameter. For a symmetric system, minimization of the free-energy difference associated with the microphase separation from a homogeneous state to the microphase separated morphology gives

$$\alpha_i = \sqrt{2} \tag{20}$$

and

$$\lambda = \frac{6T_A}{\chi Z_A} + \left[\left(\frac{6T_A}{\chi Z_A}\right)^2 + \frac{1}{6}\pi^2 t_D^2\right]^{1/2}, \tag{21}$$

where χ is the Flory–Huggins interaction parameter, Z_A is the degree of polymerization of A (assumed equal for Z_B), and t_D is the range of Debye interactions that account for the nonlocality of interactions and is assumed to be about 8 Å. Using Eqs. (16)–(21), one can, in principle, calculate the domain characteristics based on knowledge of the physical parameters of the copolymer. However, there is one adjustable parameter in the theory, ζ, whose value greatly affects the calculation for both the long period and the interfacial thickness.

Helfand and co-workers presented a theory[62–65] for block copolymer mesophases which avoids some of the approximations inherent in the confined-chain model of Meier.

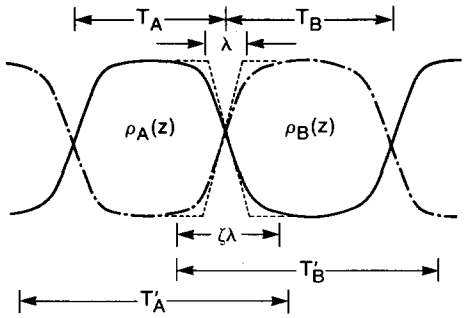

FIG. 14. Schematic diagram of the segment density profiles for a diblock copolymer as discussed by Meier (Refs. 56–59).

The essential point of departure from the confined-chain approach outlined above is the generation of the barrier and density constraints by use of a modified diffusion equation[74,75] to generate chain statistics. This is a self-consistent-field theory where an assumed polymer density pattern determines the probability distribution of the conformation of the macrodomains and these probabilities predict the assumed densities.

Application of the general theory to the problem of block copolymers[62] required a moderately difficult numerical computation. Consequently, Helfand and Wasserman[63] developed an approximation to the general theory in the narrow interface approximation limit (NIA). This is valid in the limit of high degree of polymerization where the interface is narrow compared to the domain size. They suggested[65] that the NIA is applicable for $\chi Z_i \geqslant 20$. Within the NIA the free-energy difference per molecule between the microphase-separated and phase-mixed copolymer is given by

$$\frac{\Delta F}{nkT} = \frac{2\gamma}{kT}\left(\frac{Z_A}{\rho_{0A}} + \frac{Z_B}{\rho_{0B}}\right)\frac{1}{L} + \log\left(\frac{L}{2a_J}\right) + 0.141\frac{(Z_A^{1/2}/b_A\rho_{0A})^{2.5} + (Z_B^{1/2}/b_B\rho_{0B})^{2.5}}{[(Z_A/\rho_{0A}) + (Z_B/\rho_{0B})]^{2.5}}L^{2.5} - \rho_0\chi\frac{(Z_A/\rho_{0A})(Z_B/\rho_{0B})}{(Z_A/\rho_{0A}) + (Z_B/\rho_{0B})}, \tag{22}$$

where Z_i is the degree of polymerization of block i with monomer number density ρ_{0i} and Kuhn statistical segment length b_i. γ is the interfacial tension between the domains, n is the total number of molecules, and a_J is the width around the interface where the junction points can reside.

The first term on the right-hand side of Eq. (22) is associated with the interfacial free energy which contains the interaction energy of mixing at the interface and the loss of conformational entropy due to the restriction of chain A to the A phase. This term, proportional to the surface-to-volume ratio, decreases as the size of the domains increases and tends to maximize the size of the microdomains. The theory mandates that the interface for the copolymers be identical to that between the homopolymers A and B. The interfacial behavior between the two blocks of a diblock copolymer can be estimated using the theory of Helfand and Tagami[76] for a

symmetric system or the refinement by Helfand and Sapse[77] for an asymmetric pair. For a Gaussian random walk in a mean field in the limit of infinite molecular weight they obtained[77]

$$\gamma = kT(\chi\rho_0)^{1/2}\left[\frac{\beta_A+\beta_B}{2}+\frac{1}{6}\frac{(\beta_A-\beta_B)^2}{(\beta_A+\beta_B)}\right], \quad (23)$$

where

$$\beta_i^2 = \rho_{0i}b_i^2/6. \quad (24)$$

The interfacial profile is predicted to have a hyperbolic tangent functional form

$$\rho_{0A}(z') = \frac{\rho_0}{2}[1-\tanh(2z'/a_I)] \quad (25)$$

with $z'=0$ at the middle of the interface. The interfacial thickness a_I is

$$a_I = \rho_0\left(\frac{dz'}{d\rho_{0A}}\right)_{\rho_{0A}/\rho_0=1/2} = 2\left(\frac{\beta_A^2+\beta_B^2}{2\chi\rho_0}\right)^{1/2}. \quad (26)$$

There are two sources of opposition to the domain growth. The first is related to the restriction of placement of the chemical joint between the blocks in a region of width a_J around the interface. This leads to a loss of entropy due to the joint localization which is the second term in Eq. (23). Using the density profiles appropriate to a homopolymer interface, the freedom of placement of a joint at the interface a_J is given by[63]

$$a_J = \frac{\pi}{2}\left(\frac{\beta_A\beta_B}{\chi\rho_0}\right)^{1/2}P_{1/2}\left(\frac{\beta_A^2+\beta_B^2}{2\beta_A\beta_B}\right), \quad (27)$$

where $P_{1/2}$ is the Legendre function. a_J is independent of domain size for large degrees of polymerization. An important factor that limits the growth of the domains is associated with the requirement that within the domains the density must be maintained at the bulk density. This requirement alters the spatial conformation of the molecule and causes a loss of the conformational entropy that is represented by the third term in Eq. (22). The final term of Eq. (22) is independent of L and serves to set the zero of free energy as a homogeneous mixture of the block, if such were stable. Helfand and Wasserman[65] presented a routine that, for a set of physical parameters, determines the domain spacing by performing a minimization of the free energy of Eq. (22). The equilibrium domain period L is shown to obey the equation

$$L \propto (Z_A+Z_B)^{0.64}. \quad (28)$$

The interfacial thickness is determined from Eq. (26).

Ohta and Kawasaki[67,68] used a variational method to study the statistical properties of the microphase-separated diblock copolymers in the strong segregation limit. They obtained the free-energy functional by a method similar to the one employed by Leibler[71] based on the random-phase approximation.[78,79] They emphasized that the long-range interaction of the concentration deviation is of central importance in the strong-segregation limit. Therefore, the higher-order vertex functional in the free-energy function were retained in the calculation and were calculated employing the local approximation. This was justified by showing that long-range interactions which are manifest in the quadratic term in the order parameter do not appear for n-body interactions with $n\geqslant 3$. In the narrow interface limit, they obtained the free energy per unit volume in the ordered lamellar phase as

$$F = \frac{\eta_e^2}{N}\left[\frac{2}{3}\frac{N}{L\xi}+\frac{1}{6}L^2N\alpha\phi^2(1-\phi)^2\right], \quad (29)$$

where N is the total degree of polymerization, L is the long period, ξ is a parameter related to the interfacial thickness, and ϕ is the volume fraction of the A-rich domains related to f, the fraction of A monomers in the copolymer, by

$$\phi = [\eta_e - (\tfrac{1}{2}-f)]/2\eta_e. \quad (30)$$

The interfacial profile is given by

$$\rho_i/\rho_0 = \frac{1}{2}+\eta_e\tanh\left(\frac{z'}{\xi}\right). \quad (31)$$

Therefore, the interfacial thickness a_I is given by

$$a_I' = \frac{a_I}{b} = 2\xi = \left[\frac{N}{f(1-f)\bar{\chi}}\right]^{1/2}, \quad (32)$$

where

$$\bar{\chi} = 2\rho_0N\chi - \frac{S(f)}{2f^2(1-f)^2}. \quad (33)$$

For a symmetric diblock copolymer the function $S(f)=0.9$ and ρ_0 is the average monomer number density. The parameter α in Eq. (29) is given by

$$\alpha = \frac{3}{R_g^4f(1-f)}, \quad (34)$$

where $R_g^2 = N/2$ since all lengths are given in units of the statistical segment length, b.

Minimization of the free energy with respect to L gives

$$\frac{L}{\xi} = \left[\frac{2f(1-f)}{3\phi^2(1-\phi)^2}\right]^{1/3}\left(\frac{R_g}{\xi}\right)^{4/3}. \quad (35)$$

In the limit of $\bar{\chi}\gg 1$, as is the case for our system, $\eta_e=1/2$ and $\phi=f=0.5$. It should be pointed out that the above equations differ by some numerical constants from the equation in the original paper due to algebraic errors in the original derivation.

Semenov[69] has employed an electrostatic analogue in studying the morphology of diblock copolymers in the strong segregation limit. The source of the "electric field" appears to be the junction points of the two blocks. In the case of a lamellar morphology, the period is given by

$$L = 4\left(\frac{3}{\pi^2}\right)^{1/3}\frac{b}{\sqrt{6}}N^{2/3}\chi^{1/6} \quad (36)$$

and the interfacial profile follows a hyperbolic tangent functional form with a characteristic thickness

$$a_I = \frac{2b}{\sqrt{6\chi}}. \quad (37)$$

This is exactly the same as the one predicted by Helfand and Tagami[76] for symmetric homopolymers of infinite molecular weight.

VI. COMPARISON WITH THEORY

From the preceding section, it is evident that the parameters needed for a comparison between experimental results

and theoretical predictions are the statistical segment lengths of the two blocks, b_{PS} and b_{PMMA}; the number density of monomeric units, $\rho_{0,PS}$ and $\rho_{0,PMMA}$; the Flory–Huggins interaction parameter, χ; and the degrees of polymerization Z_{PS}, Z_{PMMA}, and $N = Z_{PS} + Z_{PMMA}$. The statistical segment length for polystyrene has been reported by Ballard Wignall, and Schelten[80] from neutron scattering experiments on bulk polystyrene as 6.8 Å. The statistical segment length of PMMA has been reported by Kirste and coworkers.[81,82] as 7.4 ± 3 Å. Thus, the statistical segment lengths of both components are quite similar. In a recent neutron scattering experiment on P(*d*-*S*-*b*-MMA) diblock copolymer ($M_w = 27\,600$, $M_w/M_n = 1.08$) in the disordered state[83] an average value of $b = 6.85$ Å could quantitatively describe the results. Thus, this value will be used here for both the constituents.

The monomer number densities were calculated using literature values[84] of the densities of PS and PMMA (1.05 and 1.15 g/cm^3, respectively). The densities of perdeuterated PS and PMMA were assumed to be 1.13 and 1.24 g/cm^3, which were calculated from those of the hydrogeneous components corrected for the increase in the molecular mass upon substitution of hydrogen by deuterium. The average values of the densities were calculated from the geometric mean.[76]

The temperature dependence of the Flory–Huggins interaction parameter was determined in a small-angle neutron scattering study of disordered P(*d*-*S*-*b*-MMA) diblock copolymer and is given by[83]

$$\chi = 0.028 + 3.9/T, \tag{38}$$

where T is the absolute temperature. For the studies discussed herein, $T = 170$ °C and, therefore, $\chi = 0.0372$.

A tabulation of the experimentally measured lamellar period and the width of the interface and the corresponding calculated values are shown in Table IV. Meier's theory contains an adjustable parameter ζ related to the freedom of placing the joint in a distance $\zeta\lambda$ around the interface. In order to fix ζ, the value of the long period predicted using Eqs. (19)–(23) for the P(*d*-*S*-*b*-MMA) 100 K specimen was equated with the experimental value yielding $\zeta = 0.74$. This was then used to calculate the long periods and the interfacial widths of the remaining copolymers. The results in Table IV show that while the predicted long periods are not very different from the experimental values, the theory overestimates the interfacial widths. On the other hand, the predictions of the theory of Helfand and co-workers agree well with the experimentally measured period, but the interface thickness is underestimated by ~60%. As discussed before, in their treatment, the interfacial region between the two blocks in a diblock copolymer must be identical to that between the corresponding homopolymers. The experimental data indeed bear this out. However, the magnitudes of the interfacial widths do not agree with the data for either the copolymers or the homopolymers. The prediction of the interfacial tension between PS and PMMA homopolymers at 170 °C is 2.16 dyn/cm. This value of the interfacial tension used is higher than those measured between PMMA of molecular weight 1×10^4 and PS with molecular weights up to 5×10^4, where at 199 °C, γ(dyn/cm) is given by[55]

$$\gamma = 1.38 - \frac{725}{M_{n,PS}^{0.9}}. \tag{39}$$

The overestimation of γ leads to the underestimation of a_I. However, γ is also used in the calculation of the period where very good agreement was found. Thus, there appears to be an inconsistency in the theoretical arguments.

Recently, Broseta *et al.*[85] considered the effect of molecular weight on the interfacial properties between two homopolymers. Modification of the square gradient approach of Cahn and Hilliard[86] by these authors showed a significant dependence of the interfacial properties at moderate molecular weights. The analytic expression they obtained for the interfacial thickness is given by

$$a_I = (a_I)_H\left[1 + \ln 2\left(\frac{1}{\chi Z_A} + \frac{1}{\chi Z_B}\right)\right], \tag{40}$$

where $(a_I)_H$ is the interfacial width defined in Eq. (26) and Z_i is the degree of polymerization of component i. Inclusion of this effect into the calculations produces an increase in the interfacial width as shown in Table IV, but these are still much smaller than the experimentally observed values.

Predictions based upon the theories of Ohta and Kawasaki and Semenov are also shown in Table IV. As can be seen the values of the period agree reasonably well with the experimental results. The width of the interface, although higher than the predictions of Helfand, are still much lower than the experimentally observed values.

Therefore, it appears that none of the current theories

TABLE IV. Comparison of experiment and theories.

	Experiment		Meier		Helfand			Ohta–Kawasaki		Semenov	
Copolymer	a_I (Å)	L (Å)	a_I (Å)	L (Å)	$(a_I)_H$ [a] (Å)	a_I [b] (Å)	L (Å)	a_i (Å)	L (Å)	a_i (Å)	L (Å)
P(*S*-*b*-*d*-MMA) 30 K	50 ± 2	175	88	120	29	37	171	37	184	29	186
P(*d*-*S*-*b*-MMA) 100 K	50 ± 3	398	86	398	29	31	411	35	423	29	421
P(*S*-*b*-*d*-MMA) 120 K	48 ± 3	510	83	452	29	31	466	35	479	29	475
P(*d*-*S*-*b*-MMA) 300 K	50 ± 5	762	64	883	29	30	869	35	880	29	870

[a] $(a_I)_H$ is calculated from Eq. (23).

[b] a_I is calculated from Eq. (37).

on diblock copolymers in the strong segregation limit can quantitatively describe the experimental details of the morphology of the PS/PMMA diblock copolymer. One possible origin for the lack of agreement between theory and experiment is that the PS/PMMA pair may be unusual. For PS/PMMA the entropic contribution to χ is dominant. For most other copolymers it is the enthalpic contribution that dominates and the temperature dependence of χ is much stronger. In addition, χ may be dependent upon the molecular weight of the block copolymer and composition.[87] Neither effect has been considered in these calculations.

One final point to be made is that the P(*S-b-d*-MMA) 30 K diblock copolymer has been shown to be in the weak segregation limit. For this one case a comparison can be made to the theory of Leibler.[71] Calculations from his arguments lead to a period of 158 Å and an interfacial width of 50 Å. While the period is 10% less than the observed period, which is outside of experimental error, the ratio of the interfacial width to the period ($X_I = 2a_I/L$) is 0.63. This is in good agreement with the experimental value of 0.57. Comparisons with the higher molecular weight copolymers would be invalid since, as the data show, the copolymers are in the strong segregation limit.

VII. CONCLUSIONS

Annealing symmetric diblock copolymers of PS and PMMA above the glass transition temperature orients the lamellar microdomains parallel to the free surface of the film. The high resolution (~ 1 nm) of neutron reflectivity, in conjunction with the orientation of the lamellar microdomains parallel to the surface, has allowed a detailed study of the morphology of the copolymers as a function of the molecular weight.

It has been shown that the hyperbolic tangent function, as opposed to a linear or a cosine-squared function, most closely describes the concentration gradient at the interface between the copolymer microdomains. The effective width of the interface is found to be independent of the molecular weight of the copolymer blocks and has a value of 50 ± 3 Å. This interface has been shown to be identical to that between layers of PS and PMMA homopolymers. However, using measured values of the Flory–Huggins interaction parameter, current thermodynamic theories are not able to describe quantitatively the observed results.

ACKNOWLEDGMENTS

The authors would like to thank D. C. Miller of the IBM Almaden Research Center for performing the x-ray photoelectron spectroscopy measurements. This work was supported in part by the Department of Energy, Office of Basic Energy Sciences Grant No. DE-FG03-88ER45375.

[1] *Processing, Structure and Properties of Block Copolymers*, edited by M. J. Folker (Elsevier, New York, 1985).
[2] *Developments in Block Copolymers—1*, edited by I. Goodman (Applied Science, New York, 1982).
[3] T. Inoue, T. Soen, T. Hashimoto, and H. Kawai, J. Polym. Sci., Part A **7**, 1283 (1969).
[4] T. Hashimoto, K. Nagatoshi, A. Todo, H. Hasegawa, and H. Kawai, Macromolecules **7**, 364 (1974).
[5] T. Hashimoto, A. Todo, H. Itoi, and H. Kawai, Macromolecules **10**, 377 (1977).
[6] T. Hashimoto, M. Shibayama, and H. Kawai, Macromolecules **13**, 1237 (1980).
[7] M. Shibayama, T. Hashimoto, and H. Kawai, Macromolecules **16**, 1434 (1983).
[8] T. Hashimoto, H. Tanaka, and H. Hasegawa, Macromolecules **18**, 1864 (1985).
[9] G. Hadziioannou and A. Skoulios, Macromolecules **15**, 258 (1982).
[10] R. W. Richards and J. L. Thomason, Macromolecules **16**, 982 (1983).
[11] F. S. Bates, R. E. Cohen, and C. V. Berney, Macromolecules **15**, 589 (1982).
[12] F. S. Bates, C. V. Berney, and R. E. Cohen, Macromolecules **16**, 1101 (1983).
[13] E. L. Thomas, D. B. Alward, D. J. Kinning, D. C. Martin, D. L. Handlin, Jr., and L. J. Fetters, Macromolecules **19**, 2197 (1986).
[14] C. P. Henderson and M. C. Williams, J. Polym. Sci., Polym. Lett. Ed. **17**, 257 (1979).
[15] F. Annighöfer and W. Gronski, Colloid. Polym. Sci. **261**, 15 (1983).
[16] F. Annighöfer and W. Gronski, Makromol. Chem. **185**, 2213 (1984).
[17] R. W. Richards and J. L. Thomason, Polymer **24**, 1089 (1983).
[18] L. Leung and J. T. Koberstein, Macromolecules **19**, 706 (1986).
[19] C. P. Henderson and M. C. Williams, Polymer **26**, 2021 (1985).
[20] R. J. Spontak, M. C. Williams, and D. A. Agard, Macromolecules **21**, 1377 (1988).
[21] A. K. Rastogi and L. E. St. Pierre, J. Colloid Interface Sci. **31**, 168 (1969).
[22] H. R. Thomas and J. J. O'Malley, Macromolecules **12**, 323 (1979).
[23] P. F. Green, T. M. Christensen, T. P. Russell, and R. Jérôme, Macromolecules **22**, 2189 (1989).
[24] J. C. Wittmann, B. Lotz, F. Candau, and A. J. Kovacs, J. Polym. Sci., Polym. Phys. Ed. **20**, 1341 (1982).
[25] E. Vanzo, J. Polym. Sci., Part A **4**, 1727 (1966).
[26] E. B. Bradford and E. Vanzo, J. Polym. Sci., Part A **6**, 1661 (1968).
[27] A. Mathis, G. Hadziioannou, and A. Skoulios, Polym. Eng. Sci. **17**, 570 (1970).
[28] H. Hasegawa and T. Hashimoto, Macromolecules **18**, 589 (1983).
[29] C. S. Henkee, E. L. Thomas, and L. J. Fetters, J. Mater. Sci. **23**, 1685 (1988).
[30] K. Ishizu and T. Fukuyama, Macromolecules **22**, 244 (1989).
[31] G. Coulon, T. P. Russell, V. R. Deline, and P. F. Green, Macromolecules **22**, 2581 (1989).
[32] T. P. Russell, G. Coulon, W. R. Deline, and D. C. Miller, Macromolecules (in press).
[33] S. H. Anastasiadis, T. P. Russell, S. K. Satija, and C. F. Majkrzak, Phys. Rev. Lett. **62**, 1852 (1989).
[34] G. Coulon, D. Ausserre, and T. P. Russell, J. Phys. (Paris) (in press).
[35] S. H. Anastasiadis, I. Gancarz, and J. T. Koberstein, Macromolecules **22**, 1449 (1989).
[36] P. F. Green, T. P. Russell, R. Jérôme, and M. Granville, Macromolecules **21**, 3266 (1988).
[37] S. A. Werner and A. G. Klein, in *Neutron Scattering*, edited by D. L. Price and K. Skold (Academic, New York, 1989).
[38] O. S. Heavens, *Optical Properties of Thin Solid Films* (Dover, New York, 1965).
[39] L. G. Parratt, Phys. Rev. **54**, 359 (1954).
[40] L. Névot and P. Croce, Phys. Appl. **15**, 761 (1980).
[41] J. Als-Nielsen, in *Structure and Dynamics of Surfaces II*, edited by M. Schommers and P. von Blanckenhagen (Springer, Berlin, 1987).
[42] A. Braslau, P. S. Pershan, G. Swislow, B. M. Ocko, and J. Als-Nielsen, Phys. Rev. A **38**, 2457 (1988).
[43] E. Bouchard, B. Farnoux, X. Sun, M. Daoud, and G. Jannink, Europhys. Lett. **2**, 315 (1988).
[44] G. P. Felcher, R. O. Hilleke, R. K. Crawford, J. Haumann, R. Kleb, and G. Ostrowski, Rev. Sci. Instrum. **58**, 609 (1987).
[45] T. P. Russell, A. Karim, A. Mansour, and G. P. Felcher, Macromolecules **21**, 1890 (1988).
[46] M. L. Fernandez, J. S. Higgins, J. Penfold, R. C. Ward, C. Shackleton, and D. J. Walsh, Polymer **29**, 1923 (1988).
[47] D. W. Oxtoby and S. A. Rice, J. Chem. Phys. **76**, 5278 (1988).
[48] P. Beckman and A. Spizzichino, *The Scattering of Electromagnetic Waves from Rough Surfaces* (Pergamon, New York, 1963).
[49] S. K. Sinha, E. B. Sirota, S. Garoff, and H. B. Stanley, Phys. Rev. B **38**, 2297 (1988).
[50] P. F. Green, T. P. Russell, R. Jérôme, and M. Granville, Macromolecules

22, 908 (1989).
[51] D. T. Clark and H. R. Thomas, J. Polym. Sci., Polym. Chem. Ed. **15**, 2843 (1977).
[52] C. S. Fadley and S. A. L. Bergstrom, Phys. Lett. **35A**, 375 (1971).
[53] R. Hosemann and S. N. Bagchi, *Direct Analysis of Diffraction by Matter* (North-Holland, Amsterdam, 1962).
[54] S. Wu, *Polymer Interface and Adhesion* (Marcel Dekker, New York, 1982).
[55] S. H. Anastasiadis, I. Gancarz, and J. T. Koberstein, Macromolecules **21**, 2980 (1988).
[56] D. J. Meier, J. Polym. Sci., Part C **26**, 81 (1969).
[57] D. J. Meier, Polym. Prepr. Am. Chem. Soc. Div. Polym. Chem. **11**, 400 (1970).
[58] T. Hashimoto, M. Shibayama, H. Kawai, and D. J. Meier, Macromolecules **18**, 1855 (1985).
[59] D. J. Meier, in *Thermoplastic Elastomers—Research and Development*, edited by N. Legge, G. Holden, and H. Schroeder (Hanser, München, Germany, 1988).
[60] D. F. Leary and M. C. Williams, J. Polym. Sci., Polym. Phys. Ed. **11**, 345 (1973).
[61] C. P. Henderson and M. C. Williams, J. Polym. Sci., Polym. Phys. Ed. **23**, 1001 (1973).
[62] E. Helfand, Macromolecules **8**, 552 (1975).
[63] E. Helfand and Z. R. Wasserman, Macromolecules **9**, 879 (1976).
[64] E. Helfand and Z. R. Wasserman, Polym. Eng. Sci. **17**, 582 (1977).
[65] E. Helfand and Z. R. Wasserman, Ref. 2, p. 99.
[66] K. M. Hong and J. Noolandi, Macromolecules **14**, 727 (1981).
[67] T. Ohta and K. Kawasaki, Macromolecules **19**, 2621 (1986).
[68] K. Kawasaki, T. Ohta, and M. Kohrogui, Macromolecules **21**, 2972 (1988).
[69] A. N. Semenov, Zh. Eksp. Teor. Fiz. **88**, 1242 (1985) [Sov. Phys. JETP **61**, 733 (1985)].
[70] E. A. DiMarzio, Macromolecules **21**, 2262 (1988).
[71] L. Leibler, Macromolecules **13**, 1602 (1980).
[72] M. Olvera de la Cruz and I. C. Sanchez, Macromolecules **19**, 2501 (1986).
[73] G. H. Fredrickson and E. Helfand, J. Chem. Phys. **87**, 697 (1987).
[74] E. Helfand, Acc. Chem. Res. **8**, 295 (1975).
[75] E. Helfand, J. Chem. Phys. **62**, 999 (1975).
[76] E. Helfand and Y. Tagami, J. Chem. Phys. **56**, 3592 (1971).
[77] E. Helfand and A. M. Sapse, J. Chem. Phys. **62**, 1327 (1975).
[78] P. G. de Gennes, J. Phys. (Paris) **31**, 235 (1970).
[79] P. G. de Gennes, *Scaling Concepts in Polymer Physics* (Cornell University, Ithaca, New York, 1979).
[80] D. G. H. Ballard, G. D. Wignall, and J. Schelten, Eur. Polym. J. **9**, 965 (1973).
[81] R. G. Kirste and O. Kratky, Z. Phys. Chem. **31**, 383 (1962).
[82] R. G. Kirste, Makromol. Chem. **101**, 91 (1967).
[83] T. P. Russell, R. P. Hjelm, and P. Seeger, Macromolecules **23**, 890 (1990).
[84] *Polymer Handbook*, edited by J. Brandrup and E. H. Immergut (Wiley, New York, 1975).
[85] D. Broseta, G. H. Fredrickson, E. Helfand, and L. Leibler, Macromolecules (in press).
[86] J. W. Cahn and J. E. Hilliard, J. Chem. Phys. **28**, 258 (1958).
[87] W. C. Jung and E. W. Fischer, Makromol. Chem., Macromol. Symp. **16**, 281 (1988).